



universität
wien

MASTERARBEIT

Titel der Masterarbeit

„Polarization forces in molecular ionic liquids“

verfasst von

Michael Schmollngruber, BSc

angestrebter akademischer Grad

Master of Science (MSc)

Wien, 2013

Studienkennzahl lt. Studienblatt:

A 066 863

Studienrichtung lt. Studienblatt:

Masterstudium Biologische Chemie

Betreut von:

Univ.-Prof. Dr. Othmar Steinhauser

Danksagung

Ich möchte an dieser Stelle all jenen Menschen danken, die mir den Weg hierher durch ihre Unterstützung ermöglicht haben.

In akademischer Hinsicht gilt dieser Dank zunächst Allen am INSTITUT FÜR COMPUTERGESTÜTZTE BIOLOGISCHE CHEMIE. Besonderer Dank gilt Prof. Dr. Othmar Steinhauser, der mich stets in allen Belangen unterstützt hat und durch seine Erklärungen der theoretischen Hintergründe meiner Arbeit Vieles erhellen konnte. Gleichmaßen möchte ich Dr. Christian Schröder danken, der durch sein unermüdliches Engagement einen sehr großen Beitrag zu dieser Arbeit geleistet hat. Weiters möchte ich Prof. Dr. Stefan Boresch danken, der mit seinem ausgesprochenen Talent für Systemadministration für einen technisch reibungslosen Betrieb des Institutes Sorge getragen hat. Ebenso möchte ich Frau Gabriele Dietinger für die einwandfreie Organisation des täglichen Ablaufs im Institut danken. Großer Dank gilt auch meinen Kollegen Sonja Maurer und Daniel Braun, die mir stets mit gutem Rat, in wissenschaftlicher Hinsicht wie auch in anderen Belangen, sowie mit moralischer Unterstützung zur Seite standen. Ebenfalls hervorheben möchte ich Dr. Michael Haberler, der mir in der Anfangszeit viele wertvolle Ratschläge gegeben und mir so das Erlernen des Programmierens wesentlich erleichtert hat.

Ausgesprochen dankbar bin ich meinen Eltern sowie meinen Geschwistern Birgit, Gernot und Helmut, die mir durch Fürsorge und bedingungslose Unterstützung ein Studium überhaupt erst möglich gemacht haben.

Abstract

This work deals with polarizable molecular dynamics (MD) computer simulations of three selected ionic liquids (IL), $\text{EMIM}^+\text{BF}_4^-$, $\text{EMIM}^+\text{TfO}^-$ and $\text{BMIM}^+\text{BF}_4^-$ including the solute molecule coumarin 153 (C153). The different solvation properties of these three liquids are described by “solvation dynamics”. In this method, the dynamical response of the solvent to an electronic excitation of the solute - C153 in this case - is characterized. Various aspects of this time-dependent response of the three ILs under investigation have been analyzed.

The respective solvation response function of the three liquids was calculated from the gathered simulation data and decomposed in several ways for a detailed interpretation. The total response was separated into contributions from (i) cations and anions, (ii) permanent and induced charges and (iii) translational and non-translational motion. The latter was accomplished using a simplified multipole expansion describing the complex charge distributions of the solvent molecules only by the net charge located at the molecular center of mass and the molecular dipole moment. In addition, the sub-picosecond decay of the solvation response function was linked to the collective translational motion of the first solvation shell. Finally, the contributions to the solvation energy were resolved according to the radial distance of the interacting molecules in order to estimate the range of these interactions.

The results of this analysis were collected in a manuscript which was then submitted to *The Journal of Chemical Physics* for publication.

Zusammenfassung

Diese Arbeit beschäftigt sich mit Molekulardynamik-Simulationen (MD) von ionischen Flüssigkeiten (IL) unter Berücksichtigung atomarer Polarisierbarkeiten. Im Speziellen wurde das Lösungsmittelverhalten dreier Flüssigkeiten - $\text{EMIM}^+\text{BF}_4^-$, $\text{EMIM}^+\text{TfO}^-$ und $\text{BMIM}^+\text{BF}_4^-$ - anhand des darin gelösten Moleküls Coumarin 153 (C153) untersucht. Dabei wurden anhand einer Methode namens Solvatationsdynamik (engl. *solvation dynamics*) die dynamischen Antworten der verschiedenen Flüssigkeiten auf eine Änderung der elektrostatischen Eigenschaften von C153 bestimmt. Diese Änderung in den elektrostatischen Eigenschaft entspricht der Änderung in der molekularen Ladungsdichteverteilung durch eine elektronische Anregung.

Die aus Simulationsdaten berechnete dynamische Antwort der verschiedenen Systeme wurde in Folge in verschiedene Beiträge aufgespalten, um eine detailliertere Interpretation zu ermöglichen. Die komplette Antwort wurde (i) in Beiträge von Kationen und Anionen, (ii) in Beiträge von permanenten und induzierten Ladungen und (iii) in Beiträge von translationaler und nicht-translationaler Bewegung unterteilt. Letzteres wurde erreicht, indem die komplexe molekulare Ladungsverteilung durch die im Schwerpunkt zentrierte molekulare Gesamtladung sowie durch das molekulare Dipolmoment approximiert wurde. Zudem wurde der sub-Picosekunden Bereich der dynamischen Antwort auf die Störung mit der kollektiven translationalen Bewegung der ersten Lösungsmittelschale in Verbindung gebracht. Abschließend wurde die Solvatationsenergie noch entsprechend der intermolekularen Distanzen radial aufgetragen, um die Reichweite dieser Interaktionen zu bestimmen.

Diese Resultate wurden in einem Manuskript zusammengefasst und bei *The Journal of Chemical Physics* zur Publikation eingereicht.

Contents

1	Introduction	1
1.1	Computer simulation of soft matter	1
1.2	Polarizability	3
1.3	Room temperature ionic liquids	6
1.4	Solvation dynamics	8
	Bibliography	11
2	Polarizable solvation dynamics of coumarin C153 in ionic liquids: Components and their cross-correlations	
	(submitted to <i>The Journal of Chemical Physics</i>)	13
A	Appendix	47
A.1	Curriculum Vitae	47

1. Introduction

1.1. Computer simulation of soft matter

”Soft matter“ is a term encapsulating highly diverse types of condensed matter (e.g. liquids) sharing important properties that distinguish these substances from matter in the solid state. In general, the state of matter can be described by the free energy

$$F = U - TS, \tag{1.1}$$

with the internal energy U , the temperature T and the entropy S . In matter existing in a solid state at room temperature (293K), the energetics are largely determined by the internal energy. In soft matter both the internal energy and the entropy are of comparable size at room temperature. The main reason for this highly different behaviour thus lies within the role of entropy. In statistical mechanics, the entropy is given by

$$S = k_B \ln(\Omega), \tag{1.2}$$

where k_B is the Boltzmann constant and Ω is the phase space volume. Hence, the entropy increases with the number of the microscopic states a system can occupy. As matter in a solid state is usually organized in a very regular fashion (e.g. as crystals), the number of possible microscopic states typically is quite low. The common property shared by all types of ”soft

1. Introduction

matter” is thus a very large number of possible molecular conformations, which in turn makes the theoretical description of such substances quite challenging.

Especially matter in the liquid state is ubiquitous in biological and chemical applications and consequently has been studied extensively. The question what causes various types of condensed matter to be in a liquid state at room temperature has been of particular interest to experimenters as well as theorists. Historically, it proved to be very challenging to construct approximate theories capable of describing the properties of liquid matter, which is mainly due to the plethora of microscopic conformations such a system can occupy. Within statistical mechanics it is possible to extrapolate to the macroscopic properties of a bulk liquid from a sample of the microscopic properties at the atomic and molecular level. Generating a sufficiently large number of samples of such microscopic states of a finite number of particles is a task well-suited to computer simulation [1].

Two simulation methods are in wide use today. The Monte-Carlo method [2] achieves its goal by a so-called random walk through many possible molecular conformations, where the transition between states occurs on the basis of a Markov chain as a controlled random process. However, as the Monte-Carlo method does not preserve the principle of microscopic reversibility, the Markov time, which describes the propagation of the simulation, is not a physical concept of time and thus prohibits the study of dynamical phenomena. Nevertheless, the Monte-Carlo method is perfectly valid when studying structural properties of matter. The other major method is classical molecular dynamics (MD) simulation, where the time evolution of a given set of particles is described by solving the classical equations of motion. MD simulation inherently keeps track of time and is therefore the first choice when studying the dynamics of a liquid system over long periods of time. In fact, MD simulation is the only simulation method

providing a direct route from intermolecular interactions to the description of dynamical phenomena.

In the construction of molecular models used in computer simulations accurate parameters are paramount for achieving satisfying results. Such parameters are usually obtained experimentally or by performing quantum-mechanical calculations. Once an accurate model of a liquid is available, computer simulation offers the possibility to interpret experimental results at the molecular level. Thereby, simulation methods have become a valuable and widely used tool used in combination with experimental methods such as NMR spectroscopy, dielectric spectroscopy and fluorescence spectroscopy in a wide range of applications.

1.2. Polarizability

An important feature missing in classical MD simulations is the ability of the molecular charge distribution to quickly adapt to changes in the local environment. The atomic partial charges defining the charge distribution are kept constant and the only way for the distribution to change is via the movement of the atoms. As this motion represents only the nuclear degrees of freedom, classical MD simulation does not account for electronic degrees of freedom. There already are various approaches to overcome this limitation aiming to implement atomic polarizabilities in a reasonably feasible manner.

One method is the fluctuating charge model [3–6], where the fixed atomic partial charges are allowed to fluctuate in response to their respective local environment. One should keep in mind, though, that the net charge of the molecule has to be kept constant at all times. Thus, the fluctuations of the charges of individual atoms in a molecule are not independent of each other.

1. Introduction

Another model widely used is the so-called induced point-dipole model, where each polarizable atom in the simulation is assigned a mathematical dipole. The energy resulting from the interaction of this dipole with the local electric field is considered in the computation of the potential energy and its strength is also determined by the respective atomic polarizabilities [7].

In this work atomic polarizabilities were implemented by so-called Drude particles, also known as the charge-on-a-spring model [8]. This method introduces two new particles of virtually no mass and equal, but oppositely signed charge for each non-hydrogen atom. One of these is always located at the coordinates of the respective atom and the other is displaced by an oscillating distance \vec{d} , thereby creating an atomic dipole that can adapt to its local environment by the movement of the displaced Drude particle around the atom. The characteristic polarizability α_β of any of the different atomic species in the system is represented by the force constant k_β^δ of the bond connecting the atom β to its associated oscillating Drude particle. For practical purposes, the charges q^δ of the Drude particles are chosen to be the same for all atom types. The force constant is thus defined by

$$k_\beta^\delta = \frac{(q^\delta)^2}{4\pi\epsilon_0\alpha_\beta}. \quad (1.3)$$

The total dipole moment $\vec{\mu}_i$ of molecule i hence includes a permanent contribution $\vec{\mu}_i^{perm}$ depending on the constant atomic partial charges $q_{i\beta}$ and atomic coordinates $\vec{r}_{i\beta}$, and an induced contribution $\vec{\mu}_i^{ind}$ depending on the position of all Drude charges.

$$\vec{\mu}_i(t) = \vec{\mu}_i^{perm}(t) + \vec{\mu}_i^{ind}(t) \quad (1.4)$$

$$\vec{\mu}_i^{perm}(t) = \sum_{\beta} q_{i\beta}(\vec{r}_{i\beta}(t) - \vec{r}_i(t)) \quad (1.5)$$

$$\vec{\mu}_i^{ind}(t) = \sum_{\beta} q^{\delta} \vec{d}_{i\beta}(t) \quad (1.6)$$

Fig. 1.1 illustrates the permanent and induced contributions to the total dipole moment of an EMIM⁺ molecule. Implementing polarizability in this way can be seen as a computationally cheap alternative to rather elaborate quantum-chemical calculations. Still, any of the three methods mentioned above comes with a significant increase in computational cost.

The addition of atomic polarizabilities is a profound change to a classical MD simulation. As will be described in more detail in Chapter 2, the induced dipoles counteract the permanent ones and thereby reduce interaction energies. These effects resemble those of a solvent, as solvent molecules typically move much faster than solute molecules and dampen their interactions. Because of this, the induced dipoles are said to act like an “inner solvent”. Recent simulation studies of ionic liquids have shown that the addition of polarization forces accelerates both the translational as well as rotational dynamics [9]. Another important feature new to MD simulations including polarization forces is that otherwise apolar species now also exhibit an induced molecular dipole moment. An example for this is the anion tetrafluoroborate, BF₄[−], which will also be discussed in greater detail in Chapter 2.

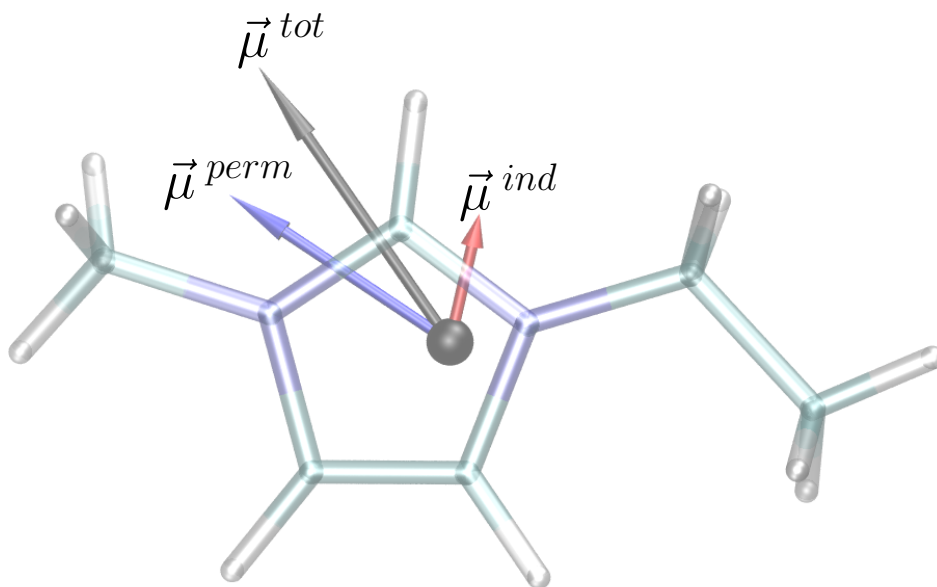


Figure 1.1.: The permanent (blue arrow) and induced (red arrow) contributions to the total molecular dipole moment (black arrow) of EMIM⁺. Throughout this work all dipole moments are referenced to the molecular center of mass (black dot).

1.3. Room temperature ionic liquids

In the past decades extensive simulation studies of the dynamical and structural properties of conventional liquids (e.g. various polar and apolar solvents) have been performed. Recent years have seen the advent of room temperature ionic liquids (IL), a novel class of solvents. An ionic liquid consists solely of charged species, but it is not to be confused with what is usually called a molten salt. The latter is solid at room temperature and is only in a liquid state at elevated temperature, whereas the former

is liquid under standard conditions for temperature and pressure. At least one of the two ionic species in a room temperature ionic liquid - usually the cation - is highly anisotropic and often also features long, flexible side chains. These properties make the formation of a regular crystal lattice much less favorable than for example in a system consisting of atomic ions. This structural anisotropy is also reflected in an anisotropic charge distribution, which causes some of the species in such liquids to exhibit rather sizeable dipole moments. The combination of a net charge and a significant dipole moment in a single molecule is a rather peculiar one. In ionic liquids, not only the rotational dynamics of the particles is strongly coupled, as it also is in conventional dipolar liquids like water, but due to the molecular net charges, the translational dynamics of the molecules also becomes highly dependent on the electrostatic interactions with a wide range of its environment, as charge-charge interactions described by the Coulomb potential exhibit a $\frac{1}{r}$ distance dependence. The strong interactions between the individual particles in ionic liquids lead to slower single-particle as well as collective dynamics than in conventional liquids, reflected in their fairly high shear viscosity (cf. Table I of Chapter 2). Another effect is that these liquids have a nearly negligible vapour pressure [10].

Besides the academic interest raised by their unique electrostatic properties, ionic liquids have also drawn attention as potential solvents for a multitude of industrial applications [11]. Due to their extremely low vapour pressure, general thermal stability over wide temperature and pressure ranges and favorable solvation properties, ionic liquids were hoped to largely replace conventional organic solvents in chemical processing, promising a more environment-friendly, “green” alternative [12–16]. Ionic liquids also offer a wide range of cations and anions that can be combined to obtain a liquid with the desired properties, be it a specific viscosity or highly specific solvation properties favouring a certain chemical reaction. So far, however,

the much higher costs and also other issues questioning their environmental harmlessness [11, 16–18] stood in the way of wide-spread use in organical synthesis and biological applications.

1.4. Solvation dynamics

A method well-suited to experimentally measure translational and rotational dynamics of a liquid sample is dielectric spectroscopy. This method measures the response of the sample to an oscillating external electric field, revealing translational and rotational dynamics on a broad frequency scale [19]. As translation and rotation in ionic liquids is strongly coupled, their dielectric spectra often are difficult to interpret. MD simulations have turned out to be a valuable tool for interpreting such spectra and retracing the experimental results to molecular movement patterns [20–22].

Solvation dynamics spectroscopy is another experimental technique for obtaining information about dynamical behaviour of a liquid sample at the molecular level. Unlike dielectric spectroscopy, it does not use an external field to probe the response of the sample. In solvation dynamics, a solute is electronically excited by a laser pulse and the time evolution of the fluorescence signal is observed. The frequency of the peak of this fluorescence signal changes over time, a phenomenon known as the Stokes shift. (cf. Fig. 2 of Chapter 2) This shift is caused by the relaxation of the solvent molecules after the abrupt change of the electrostatic properties of the solute. As such, these experiments use the solute as a probe for the evolving electric field exerted by the surrounding solvent molecules. This kind of dynamical behaviour lends itself to analysis by MD simulation. In this context, one can retrace the experimentally obtained solvation response function to molecular movement patterns in considerable detail.

This work is concerned with solvation dynamics in neat ionic liquids, specifically in 1-ethyl-3-methylimidazolium tetrafluoroborate ($\text{EMIM}^+\text{BF}_4^-$), 1-ethyl-3-methylimidazolium trifluoromethanesulfonate ($\text{EMIM}^+\text{TfO}^-$) and 1-butyl-3-methylimidazolium tetrafluoroborate ($\text{BMIM}^+\text{BF}_4^-$). Coumarin 153 (C153) has been used as a model chromophore in many experimental and computational studies and has been chosen for this study as well. Please cf. Fig. 1 of Chapter 2 for an overview of the molecular structure of all species. Chapter 2 contains a manuscript submitted to *The Journal of Chemical Physics* for publication. There, the theoretical and methodological background and also the most significant results of the analysis of these three systems are presented in a comprehensive manner.

During the course of this extensive analysis the development of new algorithms was necessary. The trajectory analysis software package GEPETTO was extended and modified to accommodate the need for new types of analysis. The focus of these additions was laid on the contributions of polarization forces and further analysis of solvation shell-resolved collective dynamical behaviour, e.g. the electric current per solvation shell \vec{J}_{cage} (cf. Eqs. 25 and 26 of Chapter 2). The definition of solvation shells was given by the already implemented Voronoi tessellation, which provides a parameterless means to define molecular neighbourhood [23]. The Voronoi polyhedra resulting from the tessellation are illustrated in Fig. 1.2, where a cross-section of the first three solvation shells of $\text{EMIM}^+\text{BF}_4^-$ surrounding C153 is shown.

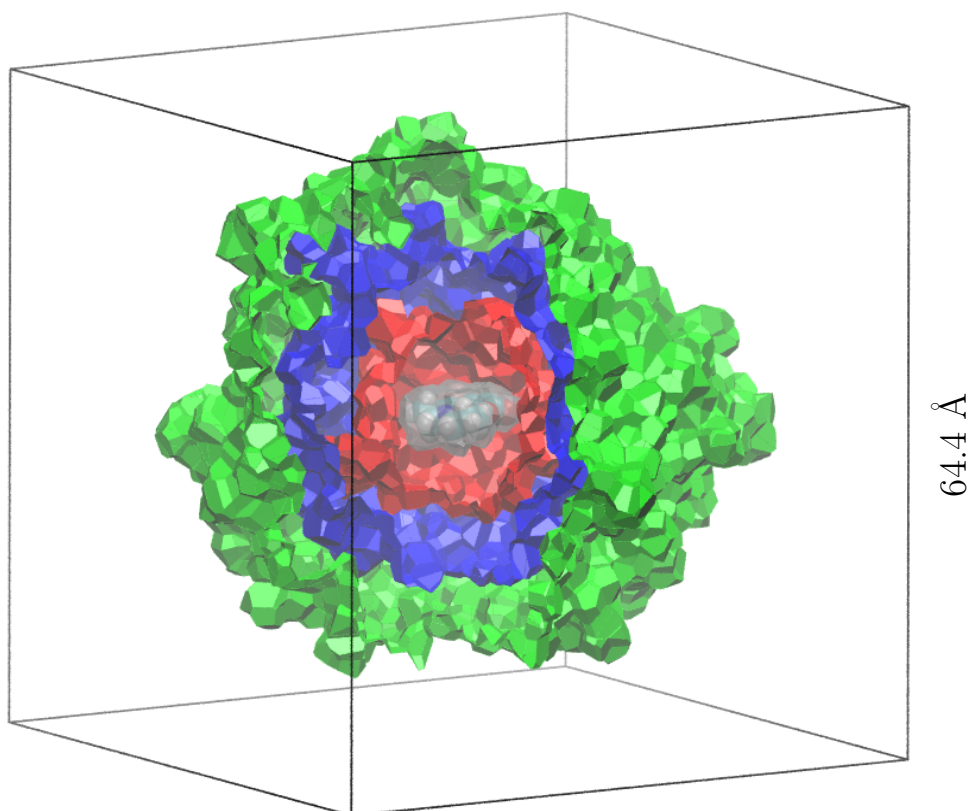


Figure 1.2.: The first three Voronoi shells of C153 in $\text{EMIM}^+\text{BF}_4^-$. The polyhedra show the surrounding surfaces of C153 (grey) and the first (red), second (blue) and third (green) solvation shells. The black lines show the edges of the simulation box. The picture was generated from a frame of a simulation of 1000 $\text{EMIM}^+\text{BF}_4^-$ ion pairs and one C153 molecule in a cubic simulation box with an edge length of 64.4 Å.

Bibliography

- [1] M. P. ALLEN and D. J. TILDESLEY, *Computer simulations of liquids*, Oxford Press, New York, 1989.
- [2] N. METROPOLIS, A. W. ROSENBLUTH, M. N. ROSENBLUTH, A. H. TELLER, and E. TELLER, *J. Chem. Phys.* **21**, 1087 (1953).
- [3] S. W. RICK, S. J. STUART, and B. J. BERNE, *J. Chem. Phys.* **101**, 6141 (1994).
- [4] S. PATEL and C. L. BROOKS III, *J. Comput. Chem.* **25**, 1 (2004).
- [5] A. K. RAPPE and W. A. GODDARD III, *J. Phys. Chem.* **95**, 3358 (1991).
- [6] J. L. BANKS, G. A. KAMINSKI, R. ZHOU, D. T. MAINZ, B. J. BERNE, and R. A. FRIESNER, *J. Chem. Phys.* **110**, 741 (1999).
- [7] T. YAN, Y. WANG, and C. KNOX, *J. Phys. Chem. B* **114**, 6886 (2010).
- [8] G. LAMOUREUX and B. ROUX, *J. Chem. Phys.* **119**, 3025 (2003).
- [9] C. SCHRÖDER and O. STEINHAUSER, *J. Chem. Phys.* **133**, 154511 (2010).
- [10] M. BIER and S. DIETRICH, *Mol. Phys.* **108**, 211 (2010).
- [11] N. V. PLECHKOVA and K. R. SEDDON, *Chem. Soc. Rev.* **37**, 123 (2008).
- [12] J. L. ANDERSON and D. W. ARMSTRONG, *Anal. Chem.* **75**, 4851 (2003).
- [13] K. R. SEDDON, *J. Chem. Tech. Biotechnol.* **68**, 351 (1997).
- [14] J. G. HUDDLESTON, A. E. VISSER, W. M. REICHERT, H. D. WILLAUER, G. A. BROKER, and R. D. ROGERS, *Green Chem.* **3**, 156 (2001).
- [15] P. WASSERSCHIED, R. VAN HAL, and A. BÖSMANN, *Green Chem.* **4**, 400 (2002).
- [16] H. ZHAO, S. XIA, and P. MA, *Journal of Chemical Technology and Biotechnology* **80**, 1089 (2005).

- [17] M. J. EARLE, J. M. S. S. ESPERANCA, M. A. GILEA, J. N. CANONGIA LOPES, L. P. N. REBELO, J. W. MAGEE, K. R. SEDDON, and J. A. WIDEGREN, *Nature* **439**, 831 (2006).
- [18] B. JASTORFF, R. STÖRMANN, J. RANKE, K. MÖLTER, F. STOCK, B. OBERHEITMANN, W. HOFFMANN, J. HOFFMANN, M. NÜCHTER, B. ONDRUSCHKA, and J. FILSER, *Green Chem.* **5**, 136 (2003).
- [19] F. KREMER and A. SCHÖNHALS, *Broadband Dielectric Spectroscopy*, Springer, Berlin, 2002.
- [20] C. SCHRÖDER, J. HUNGER, A. STOPPA, R. BUCHNER, and O. STEINHAUSER, *J. Chem. Phys.* **129**, 184501 (2008).
- [21] C. SCHRÖDER, *J. Chem. Phys.* **135**, 024502 (2011).
- [22] C. SCHRÖDER and O. STEINHAUSER, *J. Chem. Phys.* **132**, 244109 (2010).
- [23] G. NEUMAYR, C. SCHRÖDER, and O. STEINHAUSER, *J. Chem. Phys.* **131**, 174509 (2009).

**Polarizable solvation dynamics of coumarin C153 in ionic liquids:
Components and their cross-correlations**

Michael Schmollngruber, Christian Schröder,^{a)} and Othmar Steinhauser
*University of Vienna, Department of Computational Biological
Chemistry, Währingerstrasse 17, A-1090 Vienna, Austria*

Submitted to *The Journal of Chemical Physics*

The solvation dynamics of coumarin C153 dissolved in three selected molecular ionic liquids - $\text{EMIM}^+\text{BF}_4^-$, $\text{EMIM}^+\text{TfO}^-$ and $\text{BMIM}^+\text{BF}_4^-$ - was studied by molecular dynamics simulations including polarization forces. The solvation response function was decomposed with respect to permanent and induced charges, cationic and anionic contributions and translational and non-translational motions. The latter decomposition was accomplished by an appropriate multipole expansion. Furthermore, the difference in solvation energy was resolved radially. The dynamics in the sub-picosecond regime was elucidated as the mutual translational motion of the solute and the cage formed by the first solvation shell. For a qualitative interpretation, solvent molecules can be reduced to “quasi-atomic” ions carrying a net charge at their molecular center of mass. Towards a quantitative description, the dipole moment serves as a measure of charge anisotropy.

^{a)}Electronic mail: christian.schroeder@univie.ac.at

CONTENTS

I. Introduction	III
II. Theory	VI
A. Solvation response function	VI
B. Component analysis	VIII
C. Polarizability	IX
D. Species decomposition	XI
E. Multipole expansion	XI
III. Methods	XIII
IV. Results and discussion	XIV
A. Polarizability	XV
B. Species decomposition	XIX
C. Multipole expansion	XXVI
V. Conclusion	XXIX
Acknowledgement	XXX
References	XXXI

I. INTRODUCTION

Room temperature ionic liquids (IL) are a class of novel solvents that have been the subject of intense research in recent years. At the mesoscopic level their solvation properties can be characterized best by measuring their dielectric spectrum.¹ These spectra represent a superposition of collective translational and rotational motions. In a series of simulation studies we have shown how these different kinds of motion can be decomposed.^{2,3} Computational dielectric spectroscopy analyzes the response of a sample to an applied external electric field. A method that offers the opportunity to study localized solvation effects is time dependent fluorescence spectroscopy,⁴ which uses a solute as an inner probe. Upon electronic excitation following the Franck-Condon principle the charge status of the solute is changed. The subsequent reorganization of the solvent is monitored by the transient Stokes shift of the fluorescence emission frequency. The common interpretation of this shift is via the time relaxation of the difference in solvation energy upon solute excitation. The model solute most frequently used in such studies is coumarin C153.⁵⁻⁷ Therefore, we chose it as a model solute for this work.

In the past, there have been many molecular dynamics (MD) simulation studies concerned with the molecular origins of solvation dynamics in dipolar liquids.⁸⁻¹⁵ In recent years, solvation dynamics in ILs was the topic of many experimental,^{5-7,16,17} MD simulation¹⁸⁻²³ and also other theoretical^{5,24,25} studies. All previous MD studies were performed with pairwise additive forces. In this paper, we make a methodic step forward by introducing polarization forces in the solvent in order to mimic the response

of the molecular charge distribution to changes in the local environment. Since solvation spectroscopy works with a probe to analyze its local environment, we deemed the inclusion of polarization forces essential.

The solvation response function is complex in two respects. On the one hand it comprises different kinds of interactions (e.g. interaction of the solute with permanent and induced charges of the solvent molecules), on the other hand it is a superposition of various types of molecular motion. It is an intrinsic strength of simulation studies to decompose complex quantities into more elementary contributions. This paper presents a component analysis of the time correlation function underlying the interpretation of solvation dynamics. As with any decomposition procedure, cross-correlations inevitably arise. These are analyzed with special emphasis throughout this work. Actually, our decomposition is threefold.

First we separate the contributions of permanent and induced charges. A decomposition into cationic and anionic contributions follows, as was previously performed for a variety of solute/solvent combinations, e.g. a diatomic and a benzene-like model solute in EMIM^+Cl^- and $\text{EMIM}^+\text{PF}_6^-$,²⁰ a non-diffusive model solute in 1,2-dimethylimidazolium chloride¹⁸ and betaine-30²⁶ or coumarin C153¹⁹ in $\text{BMIM}^+\text{PF}_6^-$. A decomposition with respect to translational and non-translational motion completes our component analysis. However, our analysis is not based on the work of Steele²⁷ like previous works.^{8,19,28} Instead, we follow a different route exploiting the genuine features of ionic liquids. Additionally, we present a radial resolution of the solvation energy and the specific behaviour of the first solvation shell.

To achieve more general conclusions, which are not system-specific,

IV

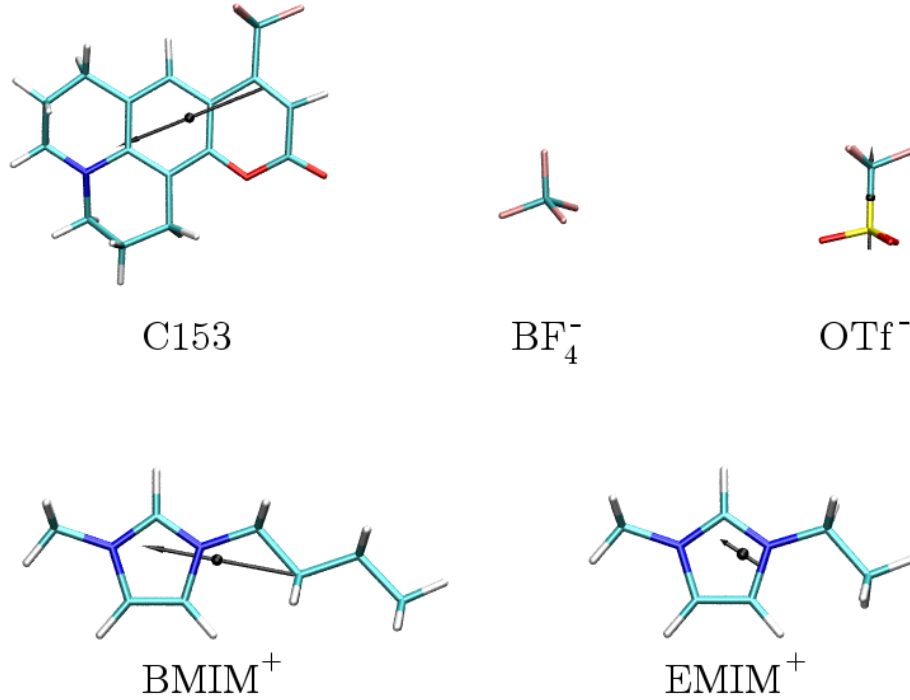


FIG. 1. Overview of the various molecular species used in the presented simulations. Black dots indicate the respective centers of mass and black arrows indicate the molecular dipole moments. In the special case of C153 the black arrow indicates $\Delta\mu$, the difference of the molecular dipole moments of ground state and excited state.

we selected the three systems 1-ethyl-3-methylimidazolium tetrafluoroborate ($\text{EMIM}^+\text{BF}_4^-$), 1-ethyl-3-methylimidazolium trifluoromethanesulfonate ($\text{EMIM}^+\text{TfO}^-$) and 1-butyl-3-methylimidazolium tetrafluoroborate ($\text{BMIM}^+\text{BF}_4^-$) with coumarin C153 as the model solute (cf. Fig. 1). $\text{EMIM}^+\text{BF}_4^-$ serves as a consensus system, as in the other two systems

either the anion or the cation was exchanged by another species with a higher dipole moment.

II. THEORY

A. Solvation response function

In experimental fluorescence spectroscopy, the normalized solvation response function is defined as

$$S_{exp}(t) = \frac{\nu(t) - \nu(\infty)}{\nu(0) - \nu(\infty)}, \quad (1)$$

with $\nu(t)$ describing the time evolution of the emission frequency and $\nu(0)$ and $\nu(\infty)$ being its limits. Theoretically this transient frequency shift is interpreted as the solvent's response to the electronic excitation of the solute molecule. In a non-equilibrium simulation, one would calculate

$$S_{neq}(t) = \frac{\overline{\Delta U(t)} - \overline{\Delta U(\infty)}}{\overline{\Delta U(0)} - \overline{\Delta U(\infty)}}, \quad (2)$$

where $\Delta U(t)$ is the difference in solvation energy between the ground state (S0) and the excited state (S1). The overbar indicates averaging over non-equilibrium trajectories. In equilibrium molecular dynamics simulations, the experimental solvation response function can be approximated within the boundaries of linear response theory. In this way, Eq. 2 can be formulated as the time correlation function (TCF)

$$C_{eq}(t) = \frac{\langle \delta \Delta U(0) \cdot \delta \Delta U(t) \rangle}{\langle \delta \Delta U^2 \rangle}. \quad (3)$$

Here $\delta\Delta U(t)$ represents the fluctuations

$$\delta\Delta U(t) = \Delta U(t) - \langle \Delta U \rangle. \quad (4)$$

In accordance with the literature,^{8,12} we compute $\Delta U(t)$ as the electrostatic interaction energy of the solute's change in charge distribution $\Delta\rho(\vec{r}, t)$ due to the electronic excitation with the electrostatic potential $\Phi(\vec{r}, t)$ of the surrounding solvent at time t .

$$\Delta U(t) = \int d\vec{r} \Delta\rho(\vec{r}, t) \Phi(\vec{r}, t) \quad (5)$$

In a fully atomistic description, the change in charge density of the solute molecule j is given by

$$\Delta\rho(\vec{r}, t) = \sum_{j\gamma} \delta(\vec{r} - \vec{r}_{j\gamma}(t)) \Delta q_{j\gamma}, \quad (6)$$

where $\Delta q_{j\gamma}$ is the difference of the partial charge of atom γ between ground and excited state. The electrostatic potential exerted by the solvent molecules i reads

$$\Phi_A(\vec{r}, t) = \sum_{i\beta} \left(\frac{q_{i\beta} - q_\delta}{|\vec{r} - \vec{r}_{i\beta}(t)|} + \frac{q_\delta}{|\vec{r} - (\vec{r}_{i\beta}(t) + \vec{d}_{i\beta}(t))|} \right), \quad (7)$$

with the atoms being indexed as β . Each atom carries an associated pair of Drude particles of charge $-2e$, the one located at the atomic coordinates $\vec{r}_{i\beta}(t)$, the other displaced by $\vec{d}_{i\beta}$. When inserting $\Delta\rho(\vec{r}, t)$ and $\Phi_A(\vec{r}, t)$ into Eq. 5, the difference in solvation energy in fully atomistic terms becomes

VII

$$\Delta U_A(t) = \sum_{j\gamma, i\beta} \left(\frac{\Delta q_{j\gamma}(q_{i\beta} - q_\delta)}{|\vec{r}_{j\gamma}(t) - \vec{r}_{i\beta}(t)|} + \frac{\Delta q_{j\gamma}q_\delta}{|\vec{r}_{j\gamma}(t) - (\vec{r}_{i\beta}(t) + \vec{d}_{i\beta}(t))|} \right). \quad (8)$$

Alternatively to the time-dependence, the solvation energy may be radially resolved as

$$\Delta U_A(r) = \frac{1}{\Delta r} \sum_{j\gamma, i\beta} \left(\frac{\Delta q_{j\gamma}(q_{i\beta} - q_\delta)}{|\vec{r}_{j\gamma} - \vec{r}_{i\beta}|} + \frac{\Delta q_{j\gamma}q_\delta}{|\vec{r}_{j\gamma} - (\vec{r}_{i\beta} + \vec{d}_{i\beta})|} \right) \delta(r - |\vec{r}_j - \vec{r}_i|) \quad (9)$$

into contributions from bins of width Δr . \vec{r}_j and \vec{r}_i refer to the centers of mass of solute and solvent molecules, respectively.

B. Component analysis

In the following sections, the complete solvation energy ΔU will be separated into two subcomponents so that

$$\Delta U(t) = \Delta U_1(t) + \Delta U_2(t). \quad (10)$$

The normalized solvation response function becomes

$$C_{tot}(t) = \frac{C_1(t) + C_2(t) + 2\chi_{12}(t)}{C_1(0) + C_2(0) + 2\chi_{12}(0)}, \quad (11)$$

where

VIII

$$C_i(t) = \langle \delta\Delta U_i(0) \cdot \delta\Delta U_i(t) \rangle_{i=1,2} \quad (12)$$

are the auto-correlation functions of the two subcomponents and

$$\chi_{12}(t) = \langle \delta\Delta U_1(0) \cdot \delta\Delta U_2(t) \rangle \quad (13)$$

is the cross-correlation function of the subcomponents.

Throughout this work, the solvation response function and all of its components were fitted to the following analytical expression, comprised of an exponential and a Kohlrausch-Williams-Watts (KWW) function:^{9,15,21}

$$C(t) \cong a_1 e^{-\left(\frac{t}{\tau_1}\right)} + a_2 e^{-\left(\frac{t}{\tau_2}\right)^\beta}. \quad (14)$$

For the Kohlrausch-Williams-Watts function an average relaxation time can be calculated as

$$\langle \tau_2 \rangle = \frac{\tau_2}{\beta} \Gamma\left(\frac{1}{\beta}\right). \quad (15)$$

C. Polarizability

From the electrostatic theorem we know that molecular charge distributions depend on the respective molecular conformations and as such change with the latter. In an heuristic way, one can model this adjustment of the molecular charge distribution to changes in the local environment by adding charge pairs, so-called Drude charges q_δ , to the frequently used set of permanent charges. In previous studies we have learned that the inclusion of these Drude charges acts as an “inner solvent”,²⁹ thereby decreasing the viscosity

of the system, which, in its turn, accelerates the dynamics. Therefore, in all systems studied here the solvent molecules were augmented by appropriate Drude charges, with the notable exception of hydrogen atoms. In order to keep the interpretation of the system manageable, we avoided even higher complexity at this point and thus, the solute molecule coumarin C153 was modeled without adding Drude charges. Otherwise we would have to abandon the concept of modeling the change in charge status upon excitation by difference charges Δq , because all Drude charges are usually taken to be the same, independent of charge status. Of course, they differ with respect to their position as a consequence of the respective polarizabilities. However, this would require to use a completely different set of polarizabilities for the excited state.

In Eq. 8 the Drude charges were included in the description of the charge distribution of the solvent molecules. Here, we separate permanent and induced contributions to the solvation energy by rewriting Eq. 8 as

$$\begin{aligned}
\Delta U_A(t) &= \Delta U_p(t) + \Delta U_i(t) \\
\Delta U_p(t) &= \sum_{j\gamma, i\beta} \frac{\Delta q_{j\gamma} q_{i\beta}}{|\vec{r}_{j\gamma}(t) - \vec{r}_{i\beta}(t)|} \\
\Delta U_i(t) &= \sum_{j\gamma, i\beta} \left(- \frac{\Delta q_{j\gamma} q_\delta}{|\vec{r}_{j\gamma}(t) - \vec{r}_{i\beta}(t)|} \right. \\
&\quad \left. + \frac{\Delta q_{j\gamma} q_\delta}{|\vec{r}_{j\gamma}(t) - (\vec{r}_{i\beta}(t) + \vec{d}_{i\beta}(t))|} \right),
\end{aligned} \tag{16}$$

thus splitting the total solvation energy ΔU_A into a permanent (ΔU_p) and an induced (ΔU_i) part. For the decomposition into permanent and

induced charges Eq. 11 becomes

$$C_{tot}^{pol}(t) = \frac{C_p(t) + C_i(t) + 2\chi^{pol}(t)}{C_p(0) + C_i(0) + 2\chi^{pol}(0)}. \quad (17)$$

D. Species decomposition

A system composed of oppositely charged species naturally lends itself to separating the solvation energy (Eq. 8) into cationic and anionic contributions

$$\Delta U_A(t) = \Delta U_+(t) + \Delta U_-(t). \quad (18)$$

Thus, the decomposition of the solvation response function (Eq. 11) becomes

$$C_{tot}^{\pm}(t) = \frac{C_+(t) + C_-(t) + 2\chi^{\pm}(t)}{C_+(0) + C_-(0) + 2\chi^{\pm}(0)}. \quad (19)$$

E. Multipole expansion

When reducing the complex anisotropic charge distribution of the various ionic solvent species to "quasi-atomic" ions carrying the net charge q_i at the molecular center of mass \vec{r}_i , the separation of the translational motion follows naturally. The multipole expansion offers a way to account for the actual anisotropy of the charge distribution. The leading term in this expansion is the molecular dipole moment and may thus be considered a measure of charge anisotropy. For an interpretation of the separation of translational and non-translational contributions to the solvation energy we use

$$\Phi_M(\vec{r}, t) = \sum_i \left(\frac{q_i}{|\vec{r} - \vec{r}_i(t)|} + \frac{\vec{\mu}_i(t) \cdot (\vec{r} - \vec{r}_i(t))}{|\vec{r} - \vec{r}_i(t)|^3} \right) \quad (20)$$

as a simplification of the electrostatic potential (Eq. 7) exerted by the solvent. Please note that the molecular dipole moment $\vec{\mu}_i$ also contains all induced effects. Inserting Eqs. 6 and 20 into Eq. 5 gives

$$\begin{aligned} \Delta U_M(t) &= \Delta U_q(t) + \Delta U_\mu(t), \\ \Delta U_q(t) &= \sum_{j\gamma, i} \frac{\Delta q_{j\gamma} q_i}{|\vec{r}_{j\gamma}(t) - \vec{r}_i(t)|} \\ \Delta U_\mu(t) &= \sum_{j\gamma, i} \frac{\Delta q_{j\gamma} \vec{\mu}_i(t) \cdot (\vec{r}_{j\gamma}(t) - \vec{r}_i(t))}{|\vec{r}_{j\gamma}(t) - \vec{r}_i(t)|^3}, \end{aligned} \quad (21)$$

For this case, equation 11 takes the special form

$$C_{tot}^M(t) = \frac{C_q(t) + C_\mu(t) + 2\chi^M(t)}{C_q(0) + C_\mu(0) + 2\chi^M(0)}. \quad (22)$$

We note that the denominator - in contrast to Eqs. 19 and 17 - may differ from the fully atomistic result $\langle (\delta \Delta U_A)^2 \rangle$, as $\Delta U_M(t)$ is only an approximation to $\Delta U_A(t)$.

Furthermore, the radial distribution of the two components of ΔU_M can be described as

$$\Delta U_q(r) = \frac{1}{\Delta r} \sum_{j\gamma, i} \frac{\Delta q_{j\gamma} q_i}{|\vec{r}_{j\gamma} - \vec{r}_i|} \delta(r - |\vec{r}_j - \vec{r}_i|) \quad (23)$$

and

$$\begin{aligned} \Delta U_\mu(r) &= \\ \frac{1}{\Delta r} \sum_{j\gamma, i} \frac{\Delta q_{j\gamma} \vec{\mu}_i(t) \cdot (\vec{r}_{j\gamma} - \vec{r}_i)}{|\vec{r}_{j\gamma} - \vec{r}_i|^3} \delta(r - |\vec{r}_j - \vec{r}_i|). \end{aligned} \quad (24)$$

XII

III. METHODS

This work presents molecular dynamics simulations of coumarin C153 in three ionic liquid solvents, EMIM⁺BF₄⁻, EMIM⁺TfO⁻ and BMIM⁺BF₄⁻ (Fig. 1). For each of these systems, two independent simulations of 1000 ion pairs and one C153 molecule were carried out. In one of these simulations, the partial charge distribution of C153 corresponded to the electronic ground state, S0, whereas in the other one, the charge distribution corresponded to the first excited state, S1. All six simulations were performed at 300 K in cubic boxes with a box length of either 64.4 Å for EMIM⁺BF₄⁻, 67.9 for EMIM⁺TfO⁻ or 68.65 Å for BMIM⁺BF₄⁻ under periodic boundary conditions. For all simulations a length of at least 50 ns was achieved using a time step of 0.5 fs. Additionally, another set of simulations with the same setup was carried out over 1 ns to collect less sparse data for analysis of short-time dynamics. Force field parameters for various species were adapted according to the following sources: EMIM⁺ (partial charges as reported by Hanke, *et al.*³⁰ all other parameters were taken from Canongia Lopes *et al.*,^{31,32}) BMIM⁺ (all parameters used as reported by Canongia Lopes *et al.*,^{31,32}) BF₄⁻ (all parameters were adopted from de Andrade *et al.*,³³) TfO⁻ (all parameters as reported by Canongia Lopes *et al.*,³⁴) C153 (partial charges as reported by Kometani *et al.*,³⁵ all other parameters were generated using SwissParam.³⁶) General simulation parameters were the same as in Ref 37: All bonds involving a hydrogen atom were kept at a constant length using the SHAKE algorithm.³⁸ Updates of non-bonded and image lists were conducted at a neighbourhood distance of 16 Å. Lennard-Jones interactions were switched off smoothly between 11 and 12 Å, while

electrostatic interactions were calculated using the PME method.^{39,40} Interactions in real space were cut off at 12 Å and the damping constant for interactions in reciprocal space was 0.410 Å⁻¹. The grid had a spacing of 1.05 Å and was interpolated using sixth-order spline functions. Polarizability of the solvent molecules was implemented through Drude oscillators on all non-hydrogen atoms. All Drude particles share a uniform charge $q^\delta = -2.0 e$ and mass $m^\delta = 0.2 amu$, both of which were subtracted from the respective atomic parameters. A more exhaustive description of the computational setup concerning the Drude oscillators was given in our previous work.^{3,29,37}

IV. RESULTS AND DISCUSSION

In previous simulation studies we have learned that viscosity governs single-particle and collective dynamics of molecular ionic liquids.⁴¹ Of the systems investigated here, EMIM⁺TfO⁻ and EMIM⁺BF₄⁻ have similar viscosities, whereas BMIM⁺BF₄⁻ is much more viscous (cf. Table I). In our simulation, this is reflected by the diffusion coefficients D and dipolar reorientational times τ listed in Table I. As all solvent molecules in our systems are polarizable, the non-polar species BF₄⁻ also exhibits a dipole moment, but of induced character. Therefore, the respective τ_{ind} describing the reorientational times of the induced part of the molecular dipole moments are listed in Table I as well. Throughout this paper, all dipole moments are referred to the center of mass of the molecule and we use the concept of a molecular dipole moment solely for interpretation.

As a validation of our computational results for solvation dynamics Fig.

TABLE I. Dynamics parameters characterizing the different systems. An overview of the presented species is given in Fig. 1.

	η_{exp}	D^+	D^-	$\langle\tau^+\rangle$	$\langle\tau^-\rangle$	$\langle\tau_{ind}^+\rangle$	$\langle\tau_{ind}^-\rangle$
	[$mPa\ s$]	[$10^{-8}cm^2s^{-1}$]	[$10^{-8}cm^2s^{-1}$]	[ps]	[ps]	[ps]	[ps]
EMIM ⁺ BF ₄ ⁻	37 (295 K) ⁴²	12.3	5.1	1237	491	653	545
EMIM ⁺ TfO ⁻	41 (298 K) ⁴³	11.1	5.2	1532	1183	758	1289
BMIM ⁺ BF ₄ ⁻	99 (295 K) ⁴²	1.9	1.6	19834	4508	12458	4580

2 presents the comparison with experimental data by Maroncelli *et al.*⁵ Taking into account all methodological differences of generating the two data sets, we consider their agreement to be quite satisfying for all three systems investigated. The observed deviation in the asymptotic regime of BMIM⁺BF₄⁻ can be traced back to the comparatively high viscosity of this system (cf. second column in Table I), which generally impairs the analysis of slow processes due to insufficient sampling. Backed by this fair agreement, computational solvation dynamics offers the possibility of a thorough threefold component analysis presented in the following sections. As validated by linear response theory, the data presented in Fig. 2, 3, 5 and 7 are averages of the ground and excited state equilibrium simulations.

A. Polarizability

A component analysis according to Eq. 17 separates contributions from permanent and Drude charges and their cross-correlation. The respective results are displayed graphically in Fig. 3. In addition, they have been

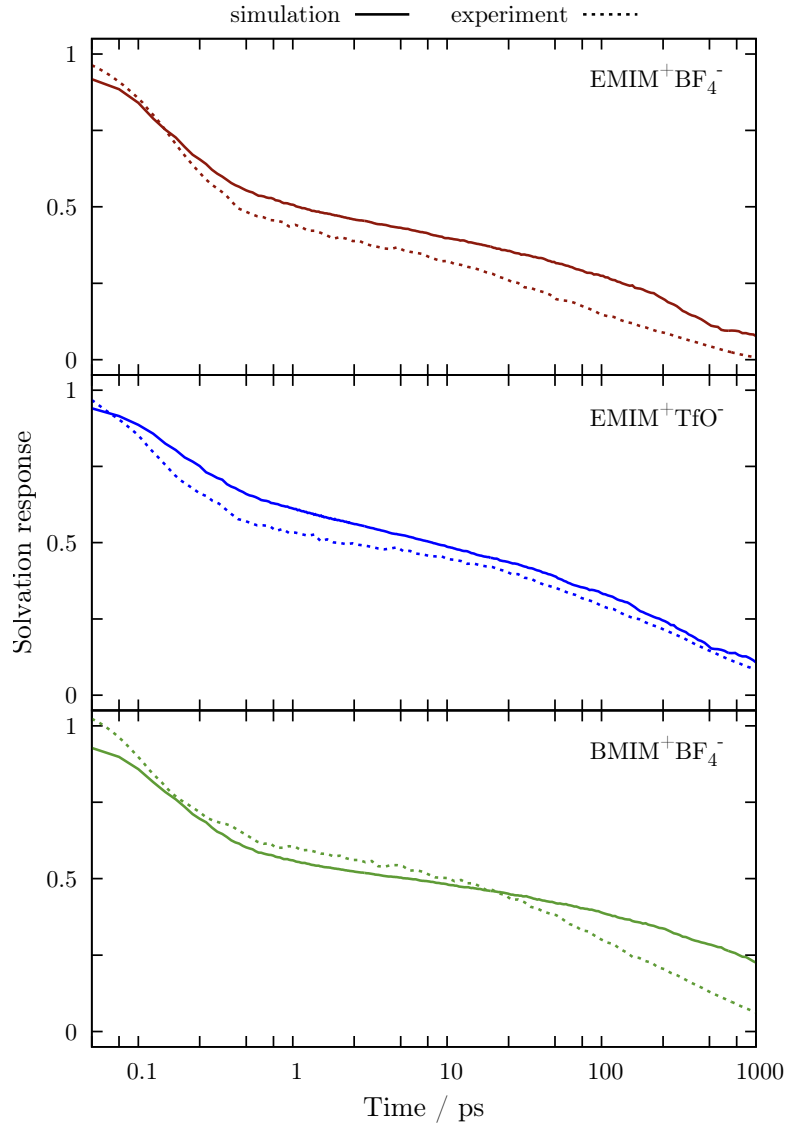


FIG. 2. Comparison of experimental⁵ and simulation (cf. Eq. 8) results for the solvation response function.

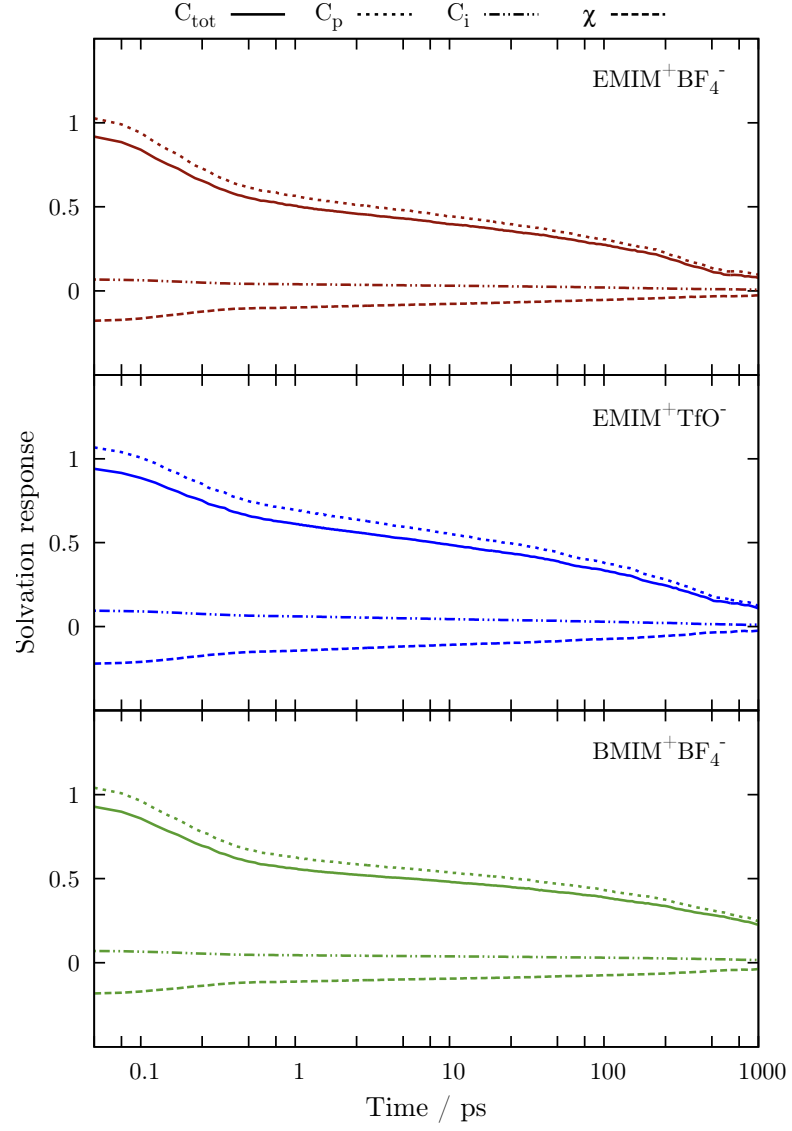


FIG. 3. Permanent and induced contributions to the solvation response function, as given by Eq. 17.

TABLE II. Stokes function fitting parameters. All functions were fitted according to Eq. 14, the average relaxation times $\langle\tau_2\rangle$ of the Kohlrausch-Williams-Watts function were calculated according to 15.

EMIM ⁺ BF ₄ ⁻					EMIM ⁺ TfO ⁻				BMIM ⁺ BF ₄ ⁻			
<i>C_{pol}</i>	<i>C_{tot}</i>	<i>C_p</i>	<i>C_i</i>	<i>2χ_{pol}</i>	<i>C_{tot}</i>	<i>C_p</i>	<i>C_i</i>	<i>2χ_{pol}</i>	<i>C_{tot}</i>	<i>C_p</i>	<i>C_i</i>	<i>2χ_{pol}</i>
<i>a</i> ₁	0.45	0.52	0.03	-0.08	0.32	0.38	0.03	-0.07	0.40	0.46	0.03	-0.08
<i>a</i> ₂	0.55	0.62	0.05	-0.12	0.68	0.77	0.08	-0.17	0.60	0.68	0.05	-0.12
<i>τ</i> ₁	0.238	0.222	0.210	0.194	0.285	0.267	0.293	0.266	0.245	0.228	0.234	0.217
<i>τ</i> ₂	216.6	215.5	167.3	198.3	226.9	225.2	87.6	162.8	1259.2	1164.1	919.2	765.5
<i>β</i>	0.40	0.37	0.33	0.28	0.37	0.37	0.28	0.31	0.31	0.31	0.30	0.33
$\langle\tau_2\rangle$	719.8	901.6	1042.9	2548.7	949.3	942.2	1125.9	1306.4	10104.3	9341.2	8512.3	4771.8
<i>C_±</i>	<i>C_{tot}</i>	<i>C₊</i>	<i>C₋</i>	<i>2χ_±</i>	<i>C_{tot}</i>	<i>C₊</i>	<i>C₋</i>	<i>2χ_±</i>	<i>C_{tot}</i>	<i>C₊</i>	<i>C₋</i>	<i>2χ_±</i>
<i>a</i> ₁	0.46	0.47	0.62	-0.64	0.33	0.36	0.36	-0.47	0.40	0.50	0.68	-0.77
<i>a</i> ₂	0.54	0.55	0.82	-0.82	0.67	1.04	0.92	-1.53	0.60	2.27	2.33	-4.02
<i>τ</i> ₁	0.242	0.285	0.259	0.282	0.340	0.361	0.339	0.405	0.244	0.330	0.302	0.34
<i>τ</i> ₂	227.5	251.1	369.6	357.0	226.0	344.9	374.1	377.4	1314.3	18044.8	6307.4	11238.3
<i>β</i>	0.40	0.37	0.37	0.37	0.49	0.44	0.41	0.44	0.32	0.39	0.44	0.46
$\langle\tau_2\rangle$	756.1	1050.6	1546.3	1493.6	469.5	899.9	1163.1	984.7	9246.7	64406.9	16456.7	26543.9
<i>C_M</i>	<i>C_{tot}</i>	<i>C_q</i>	<i>C_μ</i>	<i>2χ_M</i>	<i>C_{tot}</i>	<i>C_q</i>	<i>C_μ</i>	<i>2χ_M</i>	<i>C_{tot}</i>	<i>C_q</i>	<i>C_μ</i>	<i>2χ_M</i>
<i>a</i> ₁	0.29	0.39	0.03	-0.12	0.24	0.41	0.14	-0.31	0.23	0.31	0.07	-0.14
<i>a</i> ₂	0.71	0.88	0.11	-0.28	0.76	1.93	1.12	-2.29	0.77	1.49	0.69	-1.41
<i>τ</i> ₁	0.286	0.259	0.299	0.225	0.328	0.353	0.548	0.463	0.284	0.271	0.348	0.298
<i>τ</i> ₂	613.8	529.6	562.9	381.3	320.3	555.2	454.7	585.5	4310.6	14053.3	13682.9	29401.8
<i>β</i>	0.44	0.42	0.52	0.42	0.44	0.51	0.49	0.53	0.40	0.37	0.45	0.41
$\langle\tau_2\rangle$	1601.5	1547.1	1049.9	1113.9	835.7	1071.3	944.6	1057.6	14325.6	58796.7	33914.4	91412.5

fitted to the analytical expression in Eq. 14. The respective parameters are listed in the upper part of Table II. As a universal result, the relative contributions of these components are conserved for all three systems. This can be confirmed by the sum of the respective amplitudes (cf. the first two lines in Table II). The contribution of permanent charges exceeds the total function by typically 15% , whereas the inductive self-term is nearly

negligible. Nevertheless, the polarization forces play their role as a screening "inner solvent" by a substantial counter-active cross-term. The interplay of permanent and induced charges can be further elucidated by considering the time-averaged, but spatially resolved solvation energy defined in Eq. 9. As shown in Fig. 4, the permanent contribution extends to at least 40 Å, while the induced contribution is confined to approximately 15 Å. This may be explained by the rapid fluctuations of the Drude particles' positions, by which weaker long-range interactions are cancelled out. Viewing the Drude particles as an "inner solvent", their influence may be characterized in terms of a potential of mean force (PMF) acting between permanent charges. For this PMF an analytical expression can be given (cf. Eq. 14 of ref. 44), which points to a $1/r^6$ dependence. Thus, the range of the induced contribution is comparable to that of the traditional Lennard-Jones potential, which is usually truncated beyond 12 Å. We also note that inclusion of polarizability not only improves the results quantitatively, but also creates qualitatively new results. A striking example is the dipolar auto-correlation function of the otherwise apolar anion BF_4^- . The slight difference between the reorientational times τ^- and τ_{ind}^- listed in Table I is a consequence of molecular vibrations also resulting in a temporary dipole moment.

B. Species decomposition

Fig. 5 shows the contributions of the respective cations and anions and their cross-correlation computed according to Eq. 19. As in all other figures referring to component analysis, each set of curves is normalized to the sum

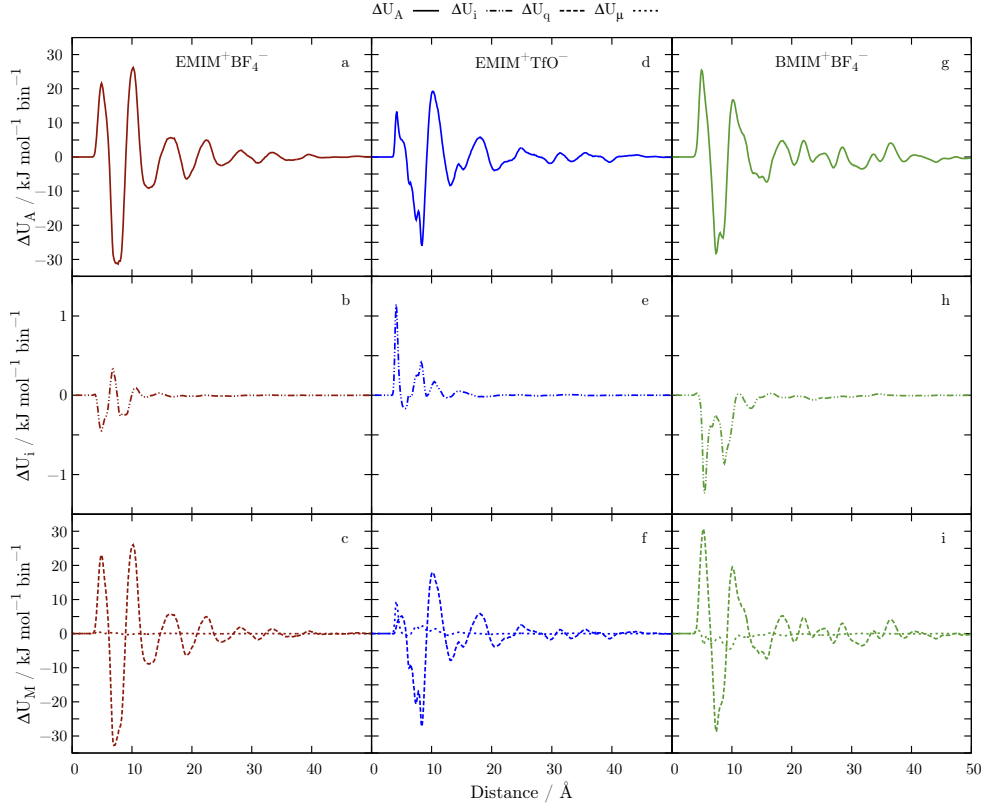


FIG. 4. ΔU radial distribution histograms, calculated with a bin width of 0.12 Å. The upper row shows the complete ΔU , the middle row only the contribution of the induced dipoles, ΔU_{ind} and the lower row shows the translational and non-translational contributions as shown in Eq. 21. Panels (a), (b) and (c) show $\text{EMIM}^+\text{BF}_4^-$, panels (d), (e) and (f) show $\text{EMIM}^+\text{TfO}^-$ and panels (g), (h) and (i) show $\text{BMIM}^+\text{BF}_4^-$.

TABLE III. Time averages and standard deviations of the solvation energy and its species-specific contributions, as defined in Eq. 18. The values are shown for both equilibrium simulations.

	ΔU_{tot}^{S0}	ΔU_{tot}^{S1}	ΔU_{+}^{S0}	ΔU_{+}^{S1}	ΔU_{-}^{S0}	ΔU_{-}^{S1}
EMIM ⁺ BF ₄ ⁻	-7.0 ± 12.9	-48.4 ± 12.8	-21.0 ± 12.1	-27.7 ± 13.0	14.0 ± 14.3	-20.7 ± 15.4
EMIM ⁺ TfO ⁻	-10.0 ± 13.2	-40.5 ± 12.3	-26.4 ± 16.0	-35.6 ± 15.3	16.5 ± 17.8	-4.9 ± 15.9
BMIM ⁺ BF ₄ ⁻	-4.8 ± 13.0	-39.9 ± 10.5	-40.8 ± 22.6	-21.8 ± 15.2	35.9 ± 22.6	-18.1 ± 16.9

of its components. Therefore, the total correlation function is normalized to unity. However, we note that the absolute initial values of the total, unnormalized solvation response functions are fairly close to each other. This can be seen from the data collected in Table III giving the average values and the standard deviations of the total and species-resolved solvation energies for both ground and excited state equilibrium simulations. The normalization factors applied in Fig. 5 are given by the square of the mean standard deviations of ground and excited state. The respective standard deviations of ΔU_{tot}^{S0} and ΔU_{tot}^{S1} are very similar and even show minimal variation for all three systems investigated.

In previous attempts to separate the cationic and anionic contributions to the solvation response function, Kobrak¹⁹ and Shim *et al.*²¹ highlighted the relative importance of the anionic over the cationic response in BMIM⁺PF₆⁻. The data presented in Fig. 5 and the fit parameters in the C_{\pm} section of Table II cannot generally confirm this argument for the systems investigated here. All three systems clearly exhibit similar behaviour of both ionic species, at least for time scales < 100 ps. We also strongly emphasize the im-

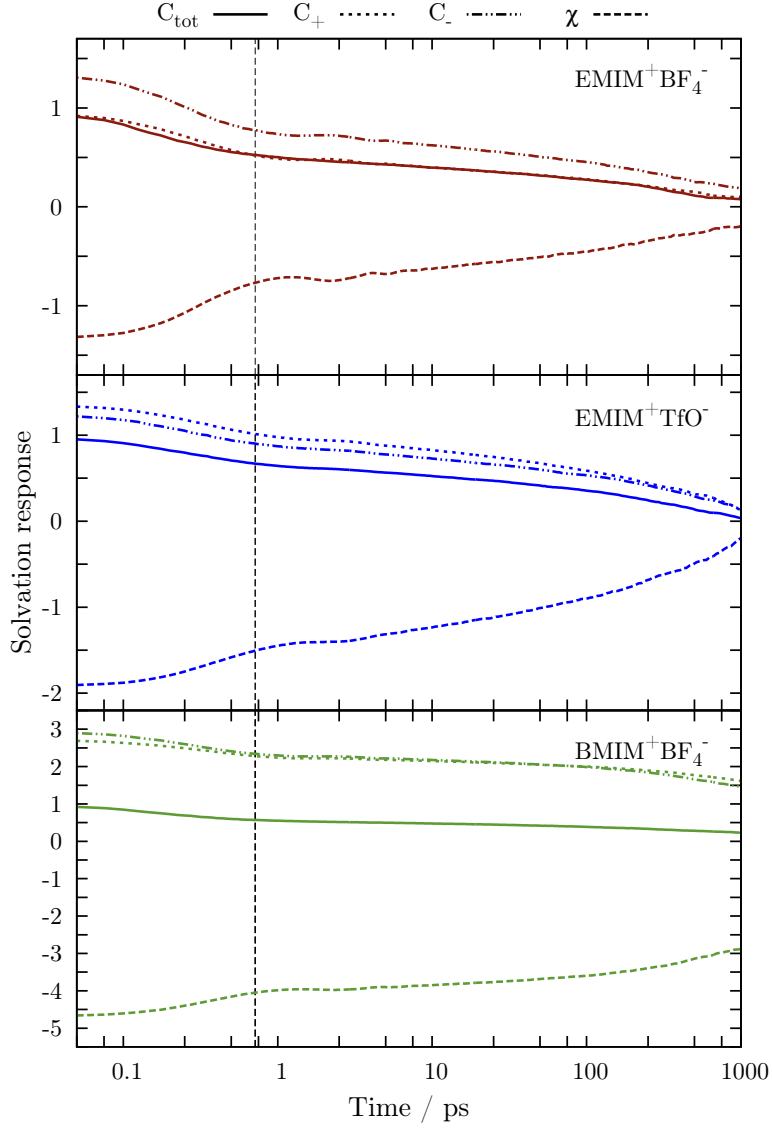


FIG. 5. Solvation response function, contributions of ionic species and cross-correlation. Panel (a) shows $\text{EMIM}^+\text{BF}_4^-$, panel (b) shows $\text{EMIM}^+\text{TfO}^-$ and panel (c) shows $\text{BMIM}^+\text{BF}_4^-$.

portance of the strong cross-correlation between cations and anions, shown as dashed lines in Fig. 5. These reflect the genuine feature of ionic liquids that the dynamics of cations and anions are very strongly coupled. In case of $\text{EMIM}^+\text{BF}_4^-$ the cross-term cancels the anionic self-term almost exactly. For $\text{EMIM}^+\text{TfO}^-$, the cationic and anionic self-terms are almost identical and the cross-term compensates more than one self-term. $\text{BMIM}^+\text{BF}_4^-$ again exhibits almost equal self-terms, but their magnitudes by far exceed the total value. Consequently, an over-compensation by the cross-term is observed. The commonly visible compensatory behaviour of cationic and anionic correlation functions has its origin in the fluctuations of the respective solvation energy time-series, which generally are perfectly synchronous, but of different sign. A second common feature of all presented correlation functions is a change in shape occurring after 1 ps. This leads to a separation into a short-time regime within the first ps and a much slower asymptotic relaxation. Up to this point, we have characterized the solvation response function and the contributions of the respective ionic species over the complete time range. Now we focus on the short-time behaviour within the first picosecond. Obviously, short-time dynamics doesn't have its roots in long-range spatial correlations, rather it has to be attributed to the interaction of the solute with its immediate neighbourhood.⁹ Our well-established Voronoi algorithm⁴⁵ offers a rational means to define immediate neighbourhood as the first Voronoi shell. Bearing in mind the mesoscopic character of experiments, we rather consider the members of a solvation shell as a collective entity instead of individual molecules. As the importance of translational motion for the sub-picosecond decay of $S(t)$ was numerously emphasized in

the literature,^{18,20} we selected the shell-specific current

$$\vec{J}_{cage}(t) = \vec{J}_{cage}^+(t) + \vec{J}_{cage}^-(t) \quad (25)$$

$$= q \left(\sum_{i=1}^{CN^+} \vec{v}_i(t) - \sum_{k=1}^{CN^-} \vec{v}_k(t) \right) \quad (26)$$

as the appropriate observable for collective translational motion of the first solvation shell with the coordination numbers CN^+ and CN^- for cations and anions, respectively. As a measure of dynamical coupling between the solute coumarin C153 and its immediate neighbourhood we computed the correlation functions $\langle \vec{v}_s(0) \cdot \vec{J}_{cage}^+(t) \rangle$ and $\langle \vec{v}_s(0) \cdot \vec{J}_{cage}^-(t) \rangle$, where $\vec{v}_s(t)$ is the translational velocity of the solute molecule. These functions are shown in Fig. 6. Since the cationic and anionic curves turned out to be of very similar shape for all systems investigated, we present the averaged curves for cations and anions. The diversity of the systems is indicated by vertical bars marking the standard deviation. The different sign of the net charge q produces mirror images of the cationic and anionic curves. The higher coordination number of cations as compared to the anions leads to somewhat higher peaks, although their ratio is smaller than CN^+/CN^- . Therefore, cationic and anionic curves do not cancel out. The most impressive feature is the common zero-crossing of all curves at 0.715 ps. It is common for all systems as well as for cations and anions. The occurrence of this zero-crossing coincides with the transition of the short-time to the long-time regime of the total solvation response function (indicated by the vertical line in Fig. 5). Furthermore, the species-specific curves C_+ and C_- show minor oscillations after this point in correspondence to oscillations in Fig. 6. Interestingly, the cross-correlation of C_+ and C_- eliminates these oscillations, making

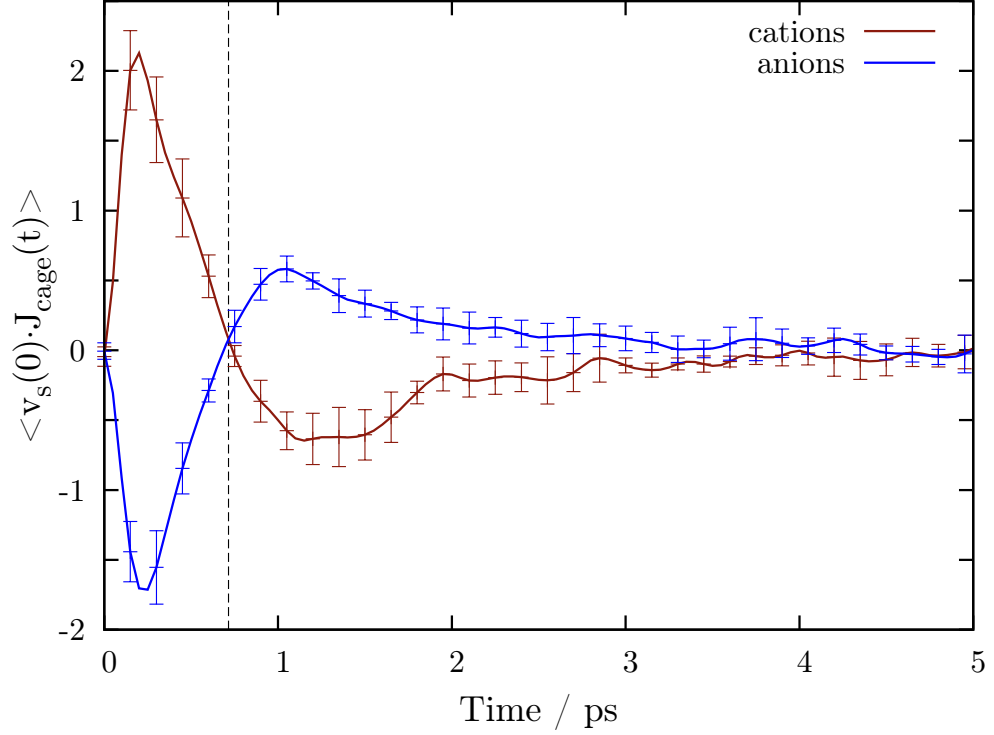


FIG. 6. Correlation functions of the molecular velocity of coumarin with the species resolved J_{cage} of all systems. The red curve is the average of all cation species, the blue curve is the average of all anion species. The bars indicate the standard deviation. The two curves intersect after 0.715 ps, indicated by the vertical black line.

the total curve monotonic. This reflects the strong coupling of collective translational motions of cations and anions within the first solvation shell. As indicated by the vertical bars in Fig. 6, the diversity of the systems investigated is remarkably small. This leads to the conclusion, that the dynamical interplay of the solute and the first solvation shell is largely

independent of the composition of the solvent. Therefore we propose the conjecture, that the short-time behaviour of solvation dynamics in an ionic liquid is largely determined by the inertial and electrostatic properties of the solute as well as the ionic character of the solvent molecules.

C. Multipole expansion

In the previous section we have learned that short-time solvation dynamics is essentially described by the solvent molecules' ionic character. In other words, the net charge plays the dominant role in short-time motion, whereas the anisotropy of the charge distribution seems to gain importance on longer time scales. Therefore, we looked for an appropriate decomposition of the solvation response function to rationalize these observations. As the change in solvation energy ΔU is described here solely by electrostatic interactions between an uncharged dipolar solute and charged dipolar solvent molecules, we considered the multipole expansion as an appropriate means of decomposition, as outlined in Eq. 21. In fact, the expansion was confined to the dipole moments, because they provided a simple, qualitative measure for the anisotropy of the charge distribution. According to Eq. 22, Fig. 7 shows the relative contributions of the charge-charge and charge-dipole interactions to the solvation response function. As a common feature of all three systems, the shape of the total curve in the short-time regime can be traced back to the charge-charge interactions, whereas the dipole moments play a minor role. This can be quantified by comparing the ratio of the respective amplitudes of the mono-exponential and the KWW part of the fit function, listed as a_1 and a_2 in lower part of Table II. In

the sequence $\text{EMIM}^+\text{BF}_4^-$, $\text{EMIM}^+\text{TfO}^-$ and $\text{BMIM}^+\text{BF}_4^-$, the respective ratios for C_q are approximately 1:2, 1:5 and 1:5 and for C_μ 1:4, 1:8 and 1:10. This is in accordance with the findings of the previous section, where the libration of the charge cage as a purely translational phenomenon was shown to cover the same time span as the initial, ultra-fast decay of the solvation response function. As the individual dipole moments of both species of $\text{EMIM}^+\text{BF}_4^-$ are either small or of inductive nature, the contribution of C_μ to the total function is marginal. Nevertheless, the cross-term substantially counteracts the dominant C_q term. Increasing the dipole moment of one species, either the cation in $\text{BMIM}^+\text{BF}_4^-$ or the anion in $\text{EMIM}^+\text{TfO}^-$, correspondingly increases the size of both C_μ and C_q . At first sight it seems surprising that the higher dipole moment also raises the charge-charge contribution C_q . However, the description of an increasingly anisotropic charge distribution in terms of an isotropic point charge becomes more insufficient as the dipole moment as a first measure of this anisotropy gains in magnitude. This is emphasized in the radially resolved multipolar contributions $\Delta U_q(r)$ and $\Delta U_\mu(r)$ to the solvation energies of the three systems given in the lower row of Fig. 4. For $\text{EMIM}^+\text{BF}_4^-$, a description in terms of net molecular charges is sufficient. Changing the cation from EMIM^+ to BMIM^+ causes a moderate, but long-range deviation between $\Delta U_q(r)$ and $\Delta U_A(r)$. The residual, however, is almost completely covered by $\Delta U_\mu(r)$, which in its turn is confined to about 15 Å, a range comparable to that of the induced contributions. The interplay of charge and dipolar contribution becomes most apparent for $\text{EMIM}^+\text{TfO}^-$, where the first peak and the subsequent shoulder of the total curve $\Delta U_A(r)$ are created by a superposition of

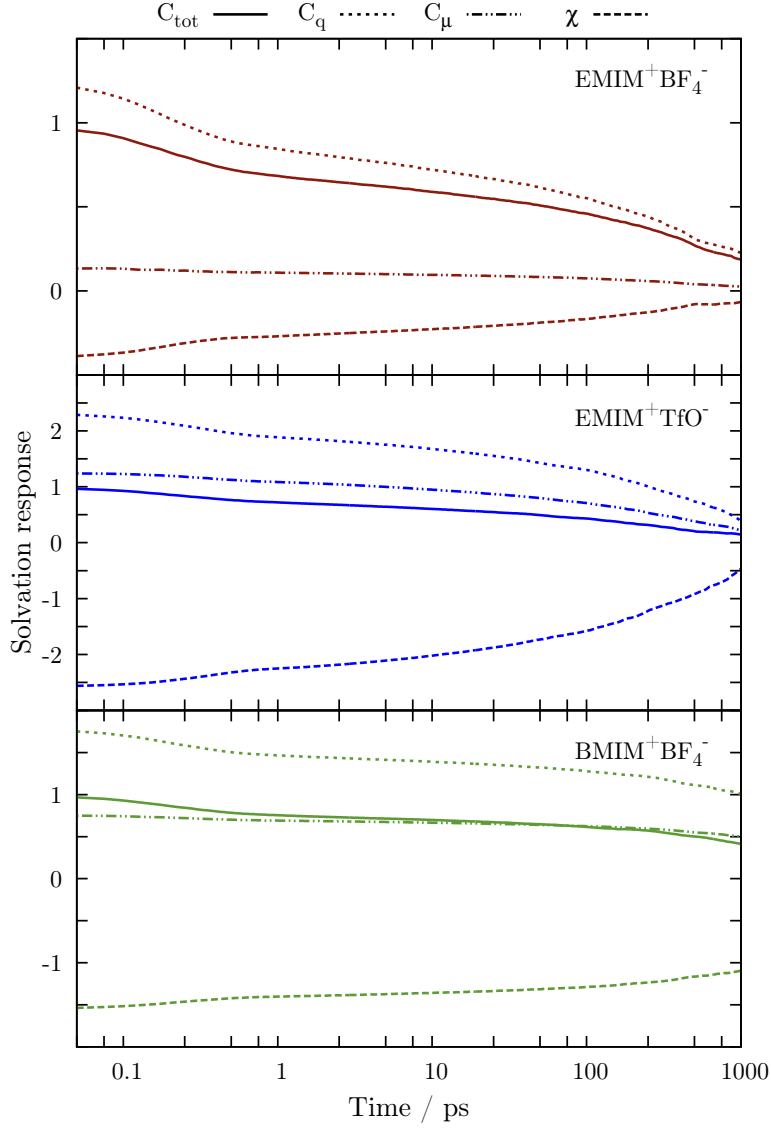


FIG. 7. Decomposition of the solvation response function according to Eq. 22. In this case, the electrostatic potential exerted by the solvent molecules is given by the multipole approximation shown in Eq. 20.

$\Delta U_q(r)$ and $\Delta U_\mu(r)$, with the latter solely accounting for the first peak and the former for the shoulder. In the sequence $\text{EMIM}^+\text{BF}_4^-$ - $\text{BMIM}^+\text{BF}_4^-$ - $\text{EMIM}^+\text{TfO}^-$, the increasing divergence between the fully atomistic view $\Delta U_A(r)$ and the picture of net molecular charges $\Delta U_q(r)$ reflects the increasingly dipolar character of the solvent molecules. While a change from EMIM^+ to BMIM^+ adds polarity to the cation, but retains the apolar anion BF_4^- , replacement of BF_4^- by TfO^- exchanges an apolar by a distinctively dipolar species. The same arguments apply to Fig. 7 previously discussed, where an increase in the spread of the individual multipolar components in the same sequence of systems can be observed.

V. CONCLUSION

In this paper we have presented simulation studies of solvation dynamics of coumarin C153 in $\text{EMIM}^+\text{BF}_4^-$, $\text{EMIM}^+\text{TfO}^-$ and $\text{BMIM}^+\text{BF}_4^-$. We have followed three concepts of partitioning the solvation energy: (i) a threefold component analysis with respect to (1) permanent and induced, (2) cationic and anionic as well as (3) translational and non-translational contributions, (ii) a radial resolution and range analysis and (iii) a focus on molecular motion in the sub-picosecond regime.

All three concepts share a common motif. For a qualitative description, the reduction of the solvent molecules to "quasi-atomic" ions carrying the net charge at the molecular center of mass is sufficient. Any quantitative deviations from the fully atomistic results can be compensated by including the dipole moment as a measure of charge anisotropy. Furthermore, the sub-picosecond region of the solvation response function is essentially

characterized by the mutual translational motion of the solute and the cage formed by the first solvation shell (Fig. 6). Again, the picture of "quasi-atomic" ions is confirmed, because all systems, despite being composed of ions considerably different in shape and charge distribution exhibited highly similar dynamics.

In addition, each pair of subcomponents turned out to be anti-correlated. This shows that the investigated effects are highly compensatory in nature, often leaving the total effect at a much smaller magnitude. Previous similar studies have shown that in polar and even more so in nonpolar liquids⁸⁻¹¹ the short-time solvation response is largely dominated by single-molecule dynamics. In contrast, as shown by the cross-correlation of the contributions of the ionic species (the dashed line in Fig. 5), the dynamics of cations and anions in ionic liquids are strongly coupled even in the sub-picosecond time scale. Our data also indicates that translational and non-translational motion in ionic liquids is strongly correlated and the extent of this correlation depends on the molecular dipole moment. It also seems that the sub-picosecond decay of the solvation response function in ionic liquids is rather determined by translational motion than by non-translational motion (cf. Fig. 7), a question that has been a topic of much discussion.^{18-20,24,25}

ACKNOWLEDGEMENT

We gratefully acknowledge the personal communication with Prof. Maroncelli, who provided us with experimental data prior to publication. We would also like to thank the Vienna Scientific Cluster (<http://www.zid.tuwien.ac.at/vsc>) of the University of Vienna, the Vienna University of Technology and the

XXX

University of Natural Resources and Applied Life Science Vienna for the generous allocation of computer time. This work was supported by Project No. P23494 of the Austrian Science Fund FWF.

REFERENCES

- ¹F. Kremer and A. Schönhal, *Broadband Dielectric Spectroscopy* (Springer, Berlin, 2002).
- ²C. Schröder and O. Steinhauser, J. Chem. Phys. **132**, 244109 (2010).
- ³C. Schröder, T. Sonnleitner, R. Buchner, and O. Steinhauser, Phys. Chem. Chem. Phys. **13**, 12240 (2011).
- ⁴M. Maroncelli, J. Mol. Liquids **57**, 1 (1993).
- ⁵M. Maroncelli, X.-X. Zhang, M. Liang, D. Roy, and N. P. Ernsting, Faraday Discuss. **154**, 409 (2012).
- ⁶P. K. Mandal, S. Saha, R. Karmakar, and A. Samanta, Curr. Science **90**, 301 (2006).
- ⁷N. Ito, S. Arzhantsev, and M. Maroncelli, Chem. Phys. Lett. **396**, 83 (2004).
- ⁸B. M. Ladanyi and M. Maroncelli, J. Chem. Phys. **109**, 3204 (1998).
- ⁹B. M. Ladanyi and R. M. Stratt, J. Phys. Chem. **99**, 2502 (1995).
- ¹⁰R. M. Stratt and M. Cho, J. Chem. Phys. **100**, 6700 (1994).
- ¹¹B. M. Ladanyi and R. M. Stratt, J. Phys. Chem. **100**, 1266 (1996).
- ¹²M. Maroncelli and G. R. Fleming, J. Chem. Phys. **89**, 5044 (1988).
- ¹³L. R. Martins, A. Tamashiro, D. Laria, and M. S. Skaf, J. Chem. Phys. **118**, 5955 (2003).
- ¹⁴P. V. Kumar and M. Maroncelli, J. Chem. Phys. **103**, 3038 (1995).

- ¹⁵S. Arzhantsev, H. Jin, G. A. Baker, and M. Maroncelli, *J. Phys. Chem. B* **111**, 4978 (2007).
- ¹⁶P. K. Chowdhury, M. Halder, L. Sanders, T. Calhoun, J. L. Anderson, D. W. Armstrong, X. Song, and J. W. Petrich, *J. Phys. Chem. B* **108**, 10245 (2004).
- ¹⁷L. S. Headley, P. Mukherjee, J. L. Anderson, R. Ding, M. Halder, D. W. Armstrong, X. Song, and J. W. Petrich, *J. Phys. Chem. A* **110**, 9549 (2006).
- ¹⁸B. L. Bhargava and S. Balasubramanian, *J. Chem. Phys.* **123**, 144505 (2005).
- ¹⁹M. N. Kobrak, *J. Chem. Phys.* **125**, 064502 (2006).
- ²⁰Y. Shim, M. Y. Choi, and H. J. Kim, *J. Chem. Phys.* **122**, 044511 (2005).
- ²¹Y. Shim, J. Duan, M. Y. Choi, and H. J. Kim, *J. Chem. Phys.* **119**, 6411 (2003).
- ²²D. Jeong, Y. Shim, M. Y. Choi, and H. J. Kim, *J. Phys. Chem. B* **111**, 4920 (2007).
- ²³M. N. Kobrak and V. Znamenskiy, *Chem. Phys. Lett.* **395**, 127 (2004).
- ²⁴H. K. Kashyap and R. Biswas, *J. Phys. Chem. B* **114**, 254 (2010).
- ²⁵S. Daschakraborty and R. Biswas, *J. Chem. Phys.* **137**, 114501 (2012).
- ²⁶V. Znamenskiy and M. N. Kobrak, *J. Phys. Chem. B* **108**, 1072 (2004).
- ²⁷W. A. Steele, *Mol. Phys.* **61**, 1031 (1987).
- ²⁸B. M. Ladanyi and S. Klein, *J. Chem. Phys.* **105**, 1552 (1996).
- ²⁹C. Schröder and O. Steinhauser, *J. Chem. Phys.* **133**, 154511 (2010).
- ³⁰C. G. Hanke, S. L. Price, and R. M. Lynden-Bell, *Mol. Phys.* **99**, 801 (2001).

- ³¹J. N. Canongia Lopes, J. Deschamps, and A. A. H. Pádua, J. Phys. Chem. B **108**, 2038 (2004).
- ³²J. N. Canongia Lopes, J. Deschamps, and A. A. H. Pádua, J. Phys. Chem. B **108**, 11250 (2004).
- ³³J. de Andrade, E. S. Böes, and H. Stassen, J. Phys. Chem. B **106**, 13344 (2002).
- ³⁴J. N. Canongia Lopes and A. A. H. Pádua, J. Phys. Chem. B **108**, 16893 (2004).
- ³⁵N. Kometani, S. Arzhantsev, and M. Maroncelli, J. Phys. Chem. A **110**, 3405 (2006).
- ³⁶V. Zoete, M. A. Cuendet, A. Grossdidier, and O. Michielin, J. Comput. Chem. **32**, 2359 (2011).
- ³⁷C. Schröder, Phys. Chem. Chem. Phys. **14**, 3089 (2012).
- ³⁸J.-P. Ryckaert, G. Ciccotti, and H. J. C. Berendsen, J. Comput. Phys. **23**, 327 (1977).
- ³⁹T. Darden, D. York, and L. Pedersen, J. Chem. Phys. **98**, 10089 (1993).
- ⁴⁰U. Essmann, L. Perera, M. L. Berkowitz, T. Darden, H. Lee, and L. G. Pedersen, J. Chem. Phys. **103**, 8577 (1995).
- ⁴¹C. Schröder and O. Steinhauser, J. Chem. Phys. **128**, 224503 (2008).
- ⁴²E. Rilo, J. Vila, J. Pico, S. García-Garabal, L. Segade, L. M. Varela, and O. Cabeza, J. Chem. Eng. Data **55**, 639 (2010).
- ⁴³H. Rodriguez and J. F. Brennecke, J. Chem. Eng. Data **51**, 2145 (2006).
- ⁴⁴G. Lamoureux and B. Roux, J. Chem. Phys. **119**, 3025 (2003).
- ⁴⁵G. Neumayr, C. Schröder, and O. Steinhauser, J. Chem. Phys. **131**, 174509 (2009).

A. Appendix

A.1. Curriculum Vitae

University of Vienna

since 03/2012 **Master thesis** (Prof. O. Steinhauser)
"Polarization forces in molecular ionic liquids"

Education

since 10/2010	Studies of biological chemistry (University of Vienna)
10/2007 - 09/2010	Studies of molecular biology (University of Vienna)
10/2006 - 09/2007	Studies of pharmacy (University of Vienna)
09/2005 - 06/2006	Military service including a training as medic
09/1997 - 06/2005	Secondary school (BG/BRG Baden Frauengasse)

Publications

- **"Polarizable solvation dynamics of coumarin C153 in ionic liquids: Components and their cross-correlations"**
M. SCHMOLLNGRUBER, C. SCHRÖDER, O. STEINHAUSER
submitted to *The Journal of Chemical Physics*
- **"The effect of Thole functions on the simulation of ionic liquids with point induced dipoles at various densities"**
T. TAYLOR, M. SCHMOLLNGRUBER, C. SCHRÖDER, O. STEINHAUSER
submitted to *The Journal of Chemical Physics*

